A Submillisecond-response Liquid Crystal for Color Sequential Projection Displays

Fenglin Peng, Haiwei Chen, Fangwang Gou, Yuge Huang and Shin-Tson Wu*
College of Optics and Photonics, University of Central Florida, Orlando, Florida 32816, USA

Abstract
We report an LC mixture with low viscosity and high clearing point (T_c~102°C) for color-sequential projection displays. Using a 1.95-μm mixed-mode twisted nematic (MTN) cell, the average gray-to-gray response time is less than 1ms, which is ~3.6X faster than the current state of the art. Such an MTN LCoS can be used for near-to-eye wearable projection displays and head-up displays in vehicles.

Keywords
Submillisecond response time; projection; color sequential; Liquid-Crystal-on-Silicon (LCoS)
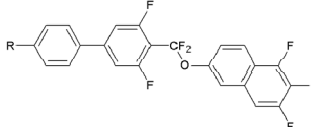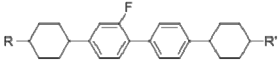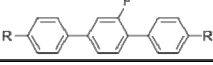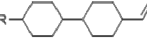
1. Introduction

Liquid-crystal-on-silicon (LCoS) has been widely used in color sequential projection displays, wearable displays and head-up displays in vehicles [1, 2]. By eliminating the color filters, both resolution density and optical efficiency are tripled. However, it requires fast response time (e.g. <1ms) to suppress color breakup and keep high image quality. To achieve submillisecond response time, several approaches have been investigated, such as 1) Employing fast response liquid crystal mode like ferroelectric liquid crystal [3] and polymer-stabilized blue phase liquid crystal [4, 5]. However, high operation voltage and low transmittance still remain to be overcome before widespread applications can be realized. 2) Using a thin vertical alignment (VA) liquid crystal cell [6]. Although it exhibits high contrast ratio, the fringing field effect degrades the transmittance, especially in a high-resolution panel [7]. On the other hand, mixed-mode twisted nematic (MTN) [8] shows several advantages for reflective LCoS projection displays, such as high transmittance, low operation voltage and weak fringing field effect. Its response time is proportional to d^2 and visco-elastic coefficient (γ_1/K_{11}). To speed up the response time of MTN mode, two approaches are considered: 1) Using a thin cell gap (d), which requires a large birefringence (Δn) LC to achieve high reflectance; 2) Employing an ultra-low viscosity LC mixture [9]. Due to thermal effect from the employed high power arc lamp or LED, the LCoS panel temperature could rise to ~35-55°C. For head-up displays inside a car, the operation temperature could easily exceed 80°C during summer time, depending on the geographic location [10, 11]. This imposes a stringent requirement on the high clearing point (T_c) of the LC candidates. To achieve high T_c, three-ring and four-ring compounds are commonly used, which dramatically increase the viscosity and lengthen the response time.

In this paper, we report a new LC mixture with high clearing point (T_c~102°C) and low viscosity. Besides, it exhibits a modest Δn and positive dielectric anisotropy (+$\Delta\varepsilon$). The physical properties are measured at different temperatures. Employing the measured material parameters in a MTN LCoS, the average gray-to-gray (GTG) rise time is 0.5 ms and decay time is 0.2 ms at T = 55°C. At T = 35°C, the corresponding GTG rise time is 1.0 ms and decay time is 0.4 ms. Promising applications for head-up vehicle displays and near-to-eye wearable projection displays are foreseeable.

2. Results and Discussion

In experiment, we collaborated with DIC (Japan) and prepared a LC mixture, designated as DIC-57F-15. Table 1 lists the chemical structures of major compounds used in the LC mixture. The homologues (different alkyl chain length R) of Compound 1 exhibits high birefringence ($\Delta n \sim 0.20$) and large dielectric anisotropy ($\Delta\varepsilon \sim 30$) [12]. The three- and four-ring compounds (Compounds 2 and 3) are added to further increase the clearing point while maintaining a high Δn. In addition, we also doped ~50 wt % non-polar diluters (i.e. Compound 4) to reduce the viscosity and activation energy. We used Differential Scanning Calorimetry (DSC, TA instrument Q100) to measure the phase transition temperatures. The melting point is below -40°C (limited by our DSC) and the clearing point is 102°C. To determine the dielectric anisotropy, we measured the capacitance of a homogeneous cell and a homeotropic cell using an HP-4274 multi-frequency LCR meter and the measured results are $\Delta\varepsilon$ = 5.0 at 25°C and 4.7 at 55°C.

Table 1. Chemical structures and major compositions of DIC-57F-15

NO.	Chemical Structures	wt %
1		~20
2		~10
3		~20
4		~50

2.1 Birefringence

Birefringence was measured through phase retardation of a homogeneous cell sandwiched between two crossed polarizers. The cell gap was controlled at ~5.05 μm by spacers. The ITO (indium tin oxide) glass substrates were over-coated with a thin polyimide (PI) layer rubbed in anti-parallel directions to create 2° pre-tilt angle and strong anchoring energy. We put the LC cell in a Linkam LTS 350 Large Area Heating/Freezing Stage controlled by TMS94 Temperature Programmer and applied a 1kHz square-wave AC voltage signal. The light sources are a tunable Argon-ion laser (λ=457 nm, 488 nm, and 514 nm) and a He-Ne laser (λ=633 nm). The transmitted light was measured by a photodiode and recorded by a LabVIEW data acquisition system. The birefringence was measured from 0–80°C at λ=633 nm as shown in Figure 1. Black squares stand for the measured data and the red line is the fitting curve using Haller's semi-

empirical equation [13]:

$$\Delta n = \Delta n_0 (1 - T / T_c)^{\beta}, \qquad (1)$$

where Δn_0 is the extrapolated birefringence at $T=0$ K and β is a material constant. $S = (1-T/T_c)^{\beta}$ is the order parameter. From the fitting, we found that Δn_0=0.15 and β=0.16.
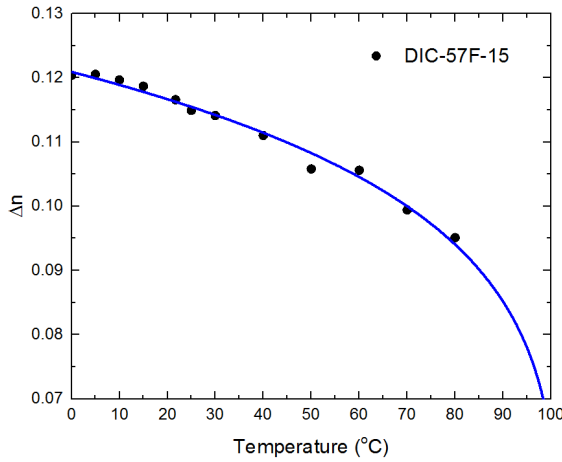

Figure 1. Temperature dependent birefringence curve at λ = 633 nm

To investigate the electro-optic performance at different wavelengths, we also measured the dispersion curve at 25°C. The results are shown in Figure 2. Black squares represent the measured data and the solid line is the fitting result with single-band birefringence dispersion model [14]:

$$\Delta n = G \frac{\lambda^2 \lambda^{*2}}{\lambda^2 - \lambda^{*2}}. \qquad (2)$$

Here G is a proportionality constant and λ^* the mean resonance wavelength. Through fitting, we obtained G=1.867μm^{-2} and λ^*=0.232μm. In principle, Δn_0 should also follow the single-band dispersion model but at a different G (denoted as G_0). From these two equations and the fitted parameters, birefringence at other wavelengths can be deduced at a specified temperature. We obtained that at T=55°C, Δn=0.105, 0.112 and 0.125 at λ=450, 550 and 650 nm; these data will be used in the simulation later.
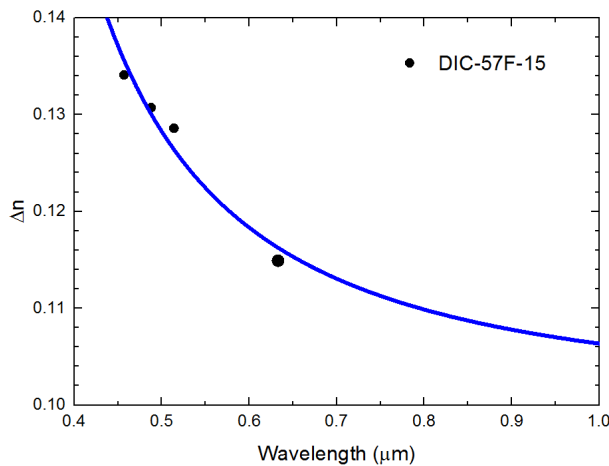

Figure 2. Birefringence dispersion curve at T=25°C.

2.2 Visco-elastic coefficient

From the response time measurement, we extracted the visco-elastic coefficient (γ_1/K_{11}) at different temperatures, as shown in Figure 3. The black squares and the red solid line represent the measured data and fitting curve, respectively. The fitting equation is expressed as:

$$\frac{\gamma_1}{K_{11}} = A \frac{\exp(E_a / k_B T)}{(1 - T / T_c)^{\beta}}. \qquad (3)$$

In Eq. (3), A is a proportionality constant, k_B is the Boltzmann constant and E_a is the activation energy. β is the material constant which has been obtained from Eq. (1). Through fitting, we obtained E_a=290 meV. Based on the fitting curve, we found that γ_1/K_{11}=2.10 ms/μm^2 at T=55°C, which is less than half of that at room temperature.
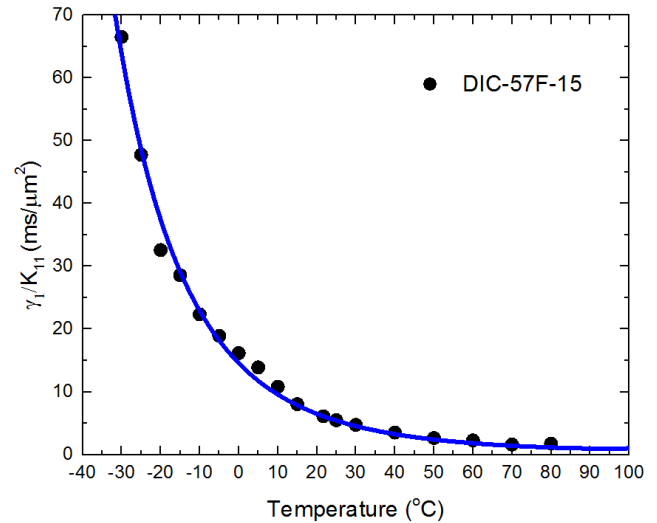

Figure 3. Temperature dependent γ_1/K_{11} of DIC-57F-15. Dots are experimental data and solid line is fitting with Eq. (3).
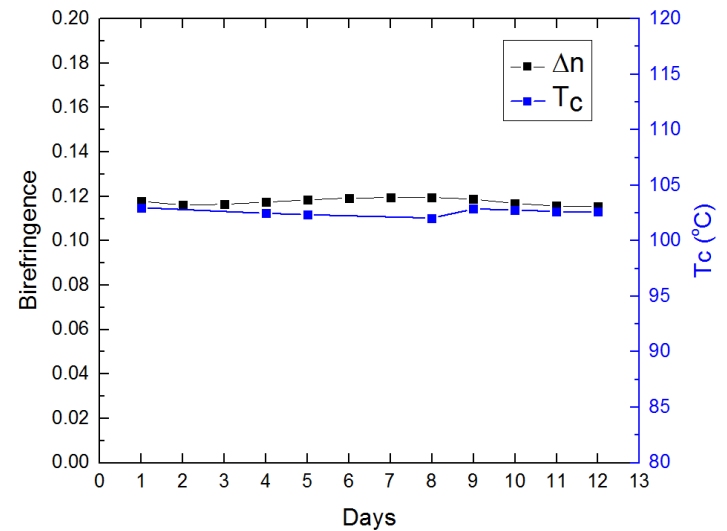

Figure 4. Birefringence and clearing point stability of DIC-57F-15. The storage temperature is controlled at T = 85°C.

2.3 Long term stability

For wearable display at outdoor or head-up display in a vehicle, the LCD panel could be exposed to sunlight or high temperature during summer time. Therefore, long term stability of liquid crystal mixture at warm environment is another concern. In an LCD panel, the employed polarizers and ITO-glass substrates help to filter out the short-wavelength UV light due to the inherent absorption. To perform accelerated reliability test, we put a bottle of DIC-57F-15 and a filled LC cell in an oven, whose temperature was controlled at $T = 85°C$ for 12 days. We took out the LC cell (and LC bottle) and measured its birefringence (Δn) at $T = 25°C$ (and clearing point) every day. Figure 4 shows the measured results during this period. The variation of birefringence is ~3% and the clearing point is less than 1%, which indicates our LC material and LC cell exhibit an excellent stability under high temperature environment. For a high-brightness LCoS projector using LED light sources, there is no UV component. The only harmful UV content comes from ambient light. Our LC structures consist of no conjugated double or triple bonds. As a result, their UV stability is superb. The only weak part is polyimide alignment layer. Therefore, for high-brightness LCoS applications we should replace the organic polyimide with inorganic alignment layers, such as SiO_x [15].
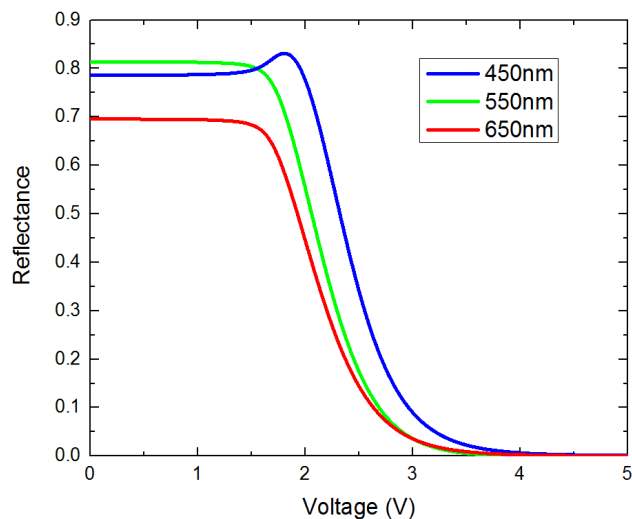

Figure 5. Simulated voltage-dependent reflectance curves at the specified RGB colors. Cell gap *d*=1.95 μm.

3. Electric-optic performance of MTN LCoS

We used a commercial LCD simulator DIMOS 2.0 to calculate the electro-optic properties of a MTN LCoS. The LC directors are twisted by 90° from top to bottom substrates (i.e. MTN 90°). In addition, other parameters were set as *d*=1.95 μm Δn=0.112 at λ=550 nm, and γ_1/K_{11} =2.10 ms/μm^2 at *T*=55°C. The angle between front LC directors and the Polarizing Beam Splitter (PBS) polarization axis is set at 20° to maximize the reflectance, and the initial pretilt angle is ~2°. MTN-90° modulates the light reflectance through both polarization rotation and phase retardation effects. A reflector is placed on the inner surface of the MTN-90° cell. For the blue and red beams, we used Δn=0.112 and 0.105 respectively to take birefringence dispersion into consideration. The voltage-dependent reflectance (VR) curves for the RGB colors are shown in Figure 5. A common good dark state is obtained at 4.5V. Thus, only a single gamma curve is needed for driving the RGB frames.

To calculate the gray-to-gray response time, we devided the VR curve at λ=550 nm into eight gray levels. The results are summerized in Table 2. Both rise time and decay time are defined as 10%-90% reflectance change. By applying overdrive voltage[16], we obtained average GTG rise time of 0.50 ms and decay time 0.20 ms. Such a fast response time helps to mitigate the color breakup of the color sequential LCoS projeciton display. For projection displays using LED light sources, the chasis temperature is around 35°C. Based on Figure 3, the extrapolated GTG rise time is 1.0 ms and decay time 0.40 ms, which are still quite fast.

Table 2. Calculated GTG response time (ms) of the MTN cell for DIC-57F-15

	1	2	3	4	5	6	7	8
1		0.23	0.30	0.37	0.46	0.56	0.71	1.00
2	0.25		0.13	0.24	0.35	0.47	0.64	0.97
3	0.29	0.08		0.12	0.23	0.37	0.55	0.94
4	0.30	0.13	0.06		0.13	0.27	0.47	0.91
5	0.31	0.17	0.10	0.05		0.15	0.36	0.90
6	0.33	0.21	0.15	0.10	0.05		0.23	0.89
7	0.36	0.25	0.20	0.15	0.11	0.07		0.92
8	0.43	0.34	0.29	0.26	0.24	0.22	0.20	

In a color-filter-embedded LCoS display [17], the applied voltage is partially shielded by the color filters. As a result, the effective voltage the LC layer experiences is lower than the applied voltage due to limited storage capacitance and voltage shielding effect [18]. Therefore, an LC mixture with slightly higher dielectric anisotropy ($\Delta\varepsilon\approx$8-10) would help lower the on-state voltage, which in turn leads to a higher contrast ratio. However, as the dielectric anisotropy increases, the rotational viscosity of the LC increases linearly, assuming the T_c and Δn remain approximately the same [11]. Therefore, employing LCs with a larger Δ helps to reduce operation voltage and increase contrast ratio, but the tradeoff is slower response time, especially at low temperatures.

4. Conclusion

A high performance LC mixture with high T_c, low viscosity, modest Δn and $\Delta\varepsilon$, excellent long-term stability is reported. This mixture is developed by DIC, and will be commercially available soon. Using the LC mixture, the MTN LCoS shows sub-millisecond response time at an elevated temperature, which enables color sequential projection display with negligible color breakup and suppressed fringing field effects. By eliminating the spatial color filters, both resolution density and optical efficiency are tripled. As a result, this device can be used for near-to-eye wearable projection displays and head-up displays in vehicles.

5. Acknowledgments

6. References

[1] E. H. Stupp, M. S. Brennesholtz. *Projection Displays,* John Wiley & Sons Inc; 1999.

[2] K. H. Fan-Chiang, C. C. Yen, C. H. Wu, C. J. Chen, B. J. Liao, Y. Y. Ho, C. Y. Liu, Y. C. Chen. "LCoS panel using novel color sequential technology," SID Symposium Digest of Technical Papers **38**(1), 150-153 (2007).

[3] V. Chigrinov, A. Srivastava, E. Pozhidaev, G. Qi, M. Ying, H. S. Kwok. "Fast high resolution ferroelectric liquid

crystal displays," SID Int. Symp. Digest Tech. Papers **45**(1), 90-92 (2014).

[4] L. Rao, S. He, S.-T. Wu. "Blue-phase liquid crystals for reflective projection displays," Journal of Display Technology **8**(10), 555-558 (2012).

[5] F. Peng, Y. Chen, J. Yuan, H. Chen, S.-T. Wu, Y. Haseba. "Low temperature and high frequency effects on polymer-stabilized blue phase liquid crystals with large dielectric anisotropy," Journal of Materials Chemistry C **2**(18), 3597-3601 (2014).

[6] Y. Chen, F. Peng, S.-T. Wu. "Submillisecond-response vertical-aligned liquid crystal for color sequential projection displays," Journal of Display Technology **9**(2), 78-81 (2013).

[7] K.-H. Fan-Chiang, S.-T. Wu, S.-H. Chen. "Fringing-field effects on high-resolution liquid crystal microdisplays," Journal of Display Technology **1**(2), 304 (2005).

[8] S. T. Wu, C. S. Wu. "Mixed-mode twisted nematic liquid crystal cells for reflective displays," Applied Physics Letters **68**(11), 1455-1457 (1996).

[9] H. Chen, M. Hu, F. Peng, J. Li, Z. An, S.-T. Wu. "Ultra-low viscosity liquid crystal materials," Optical Materials Express **5**(3), 655-660 (2015).

[10] M. Schadt, M. Petrzilka, P. Gerber, A. Villiger, G. Trickes. "New liquid crystal materials; physical properties and performance in displays for automobile, high information density and guest-host applications," Molecular Crystals

and Liquid Crystals **94**(1-2), 139-153 (1983).

[11] F. Peng, Y. Huang, F. Gou, M. Hu, J. Li, Z. An, S.-T. Wu. "High performance liquid crystals for vehicle displays," Optical Materials Express **6**(3), 717-726 (2016).

[12] H. Takatsu. "Advanced liquid crystal materials for active matrix displays," Conference Proceedings of Advanced Display Materials and Devices, p.43 (2014).

[13] I. Haller. "Thermodynamic and static properties of liquid crystals," Progress in solid state chemistry **10**, 103-118 (1975).

[14] S.-T. Wu. "Birefringence dispersions of liquid crystals," Physical Review A **33**(2), 1270-1274 (1986).

[15] C. H. Wen, S. Gauza, S. T. Wu. "Photostability of liquid crystals and alignment layers," Journal of the Society for Information Display **13**(9), 805-811 (2005).

[16] S. T. Wu. "Nematic liquid crystal modulator with response time less than 100 μs at room temperature," Applied Physics Letters **57**(10), 986-988 (1990).

[17] Y. W. Li, K. H. Fan-Chiang, C. T. Wang, T. C. Yeh, H. C. Kuo, H. C. Tsai. "LCOS using a fringe-field color filter," SID Symposium Digest of Technical Papers **43**(1), 914-917 (2012).

[18] M. Jiao, Z. Ge, Q. Song, S.-T. Wu. "Alignment layer effects on thin liquid crystal cells," Applied Physics Letters **92**(6), 061102 (2008).